Available online at www.sciencedirect.com

ScienceDirect

Procedia IUTAM 26 (2018) 14–29

Procedia IUTAM

www.elsevier.com/locate/procedia

IUTAM Symposium Wind Waves, 4-8 September 2017, London, UK

Progress in Operational Wave Forecasting

Peter A.E.M. Janssen[a], Jean-Raymond Bidlot[a]

[a]*E.C.M.W.F., Shinfield Park, Reading RG2 9AX, U.K.*

Abstract

Progress in operational sea state forecasting is discussed in the context of the energy balance equation. This fundamental law describes the evolution of the wave spectrum due to adiabatic processes such as advection and refraction and due to physical processes such as generation of waves by wind, nonlinear interactions and wave dissipation. Progress in wave prediction is illustrated by means of a verification of operational wave height forecasts against wave height observations from buoys over the last 25 years of operational practice. Verification of modelled spectra against observed spectra by buoys is shown as well.

At the moment a number of weather forecasting centres spend a considerable amount of effort in the development of a fully comprehensive coupled atmosphere, ocean-wave, ocean circulation, sea-ice model. Central in the coupling of atmosphere and ocean in the ECMWF earth system model (see e.g. [1]) are the ocean waves that determine the momentum and energy transfer across the sea surface. In this paper we therefore concentrate of the sea-state dependence of the momentum (and heat) fluxes by studying in some detail the wind input source function of the energy balance equation. The importance of the strong coupling between wind and waves is illustrated by means of impact studies.

Peer-review under responsibility of the scientific committee of the IUTAM Symposium Wind Waves.

Keywords: Type your keywords here, separated by semicolons ;

1. Introduction.

The fundamental law for wave prediction, namely the energy balance equation, describes the evolution of the wave spectrum due to adiabatic processes such as advection and refraction and due to physical processes such as generation of waves by wind, nonlinear interactions and wave dissipation. In this context, progress in operational wave prediction is discussed using verification results of forecast wave height against wave height observations from buoys. Also, evidence is presented that modelled spectral shape has improved over the past 20 years.

At ECMWF, the development of a first version of a fully comprehensive coupled atmosphere, ocean-wave, ocean circulation, sea-ice model is near completion. Presently, the interactions between the several components are as follows: Momentum loss from the atmosphere depends on the sea state following the approach of Janssen ([2], [3]). The

* Peter Janssen. Tel.: +44-1189499216; fax: +0-000-000-0000.
E-mail address: p.janssen@ecmwf.int

2210-9838
Peer-review under responsibility of the scientific committee of the IUTAM Symposium Wind Waves.
10.1016/j.piutam.2018.03.003

ocean circulation is driven by the sea state dependent stresses and produces surface currents, which are returned to the ocean-wave model and the atmospheric model needed for wave-current interaction and momentum flux. In addition, we have introduced effects of Stokes-Coriolis forcing, while the ocean circulation model is driven by momentum and energy fluxes directly from the wave model [4].

In this paper we concentrate in some detail on the wind input source function and its role in the interaction of atmosphere and ocean. It turns out that the wind input allows for a strong interaction between wind and waves. The reason for this is that while the ocean waves grow because they receive momentum from the sheared airflow, in turn the wind profile changes because the growing waves have removed momentum from the airflow. The momentum transfer from wind to waves may be so large that the associated wave-induced stress becomes a substantial fraction of the turbulent stress. Therefore, the velocity profile over sea waves is controlled by both turbulent and wave-induced momentum flux. Over a flat surface the profile of turbulent wind is usually logarithmic, but in the presence of growing wind waves deviations from the classical wind profile are to be expected. In addition, the momentum transfer from the air to the waves will be affected by the sea state, in other words one expects a strong interaction between the turbulent boundary layer and the surface waves. The importance of this process for wind and wave forecasting is illustrated by means of impact studies. Furthermore, it turns out that not only the momentum transfer, but also the heat transport is affected by the sea state, giving, again using impact studies, quite large changes in the (Tropical) circulation.

Therefore, the programme of the paper is as follows. We briefly introduce the subject of ocean wave forecasting, which is mainly about a statistical description of the sea state using the 2D wave spectrum. Improvement of ocean wave forecasting skill is illustrated by comparing forecast results with buoy observations for different years. Finally, we discuss in some detail the wind input source function which describes the generation of ocean waves by wind, and the consequent slowing down of the airflow. Consequences of the sea state dependence of momentum and heat transfer of weather and wave forecasting are briefly presented.

2. Ocean Waves.

Wave forecasting took off as an important subject when knowledge of the sea state was required for numerous landing operations during the second World War, for D-Day for example. From then onwards there followed a rapid development because of improved weather forecasting (better surface winds), an enormous increase in the number of observations (from buoys and satellites) and faster and bigger computers. From the beginning it was clear, however, that the sea state was so complicated that only a prediction of the average sea state at a location of interest was possible. Example of forecast parameters are the average wave height, the average period of the waves, and the wave spectrum.

In a statistical description of ocean waves the sea state is represented by the wave spectrum $F = F(\mathbf{k}, \mathbf{x}, t)$. Here $\mathbf{k}$ is the wavenumber vector, such that $k = 2\pi/\lambda$ with λ the wave length.

The spectrum is normalized in such a way that the integral over the spectrum gives, apart from a factor $\rho_w g$ (with ρ_w the water density and g acceleration of gravity), the wave energy:

$$\int \mathrm{d}\mathbf{k} F(\mathbf{k}) = \frac{E}{\rho_w g}, \; E = \rho_w g \langle \eta^2 \rangle$$

where η denotes the surface elevation. Thus, the wave spectrum is normalized so that it equals the wave variance $\langle \eta^2 \rangle$.

In order to establish a connection with the common practice to think in terms of wave heights (for a single wave this is the distance between crest and trough), we use the concept of significant wave height. This is a statistical measure, defined as

$$H_S = 4\sqrt{\langle \eta^2 \rangle}.$$

In a similar vein, other variables may be defined using the spectrum, e.g. mean frequency, mean wave direction, wave steepness, etc.

For ocean waves, the fundamental quantity is the action density spectrum $N(\mathbf{k}, \mathbf{x}, t)$, because it is an adiabatic invariant. Given N, the energy spectrum F then follows from

$$F(\mathbf{k}) = \frac{\sigma(\mathbf{k}) N(\mathbf{k})}{g}$$

with σ the intrinsic frequency for a gravity wave in water of depth D, while the dispersion relation for angular frequency ω reads

$$\omega = \sigma(k, D) + \mathbf{k} \cdot \mathbf{U}, \ \sigma = \sqrt{gk \tanh(kD)},$$

where $\mathbf{U}$ is the surface current.

From first principles (see [5]) one finds the following evolution equation for the action density spectrum $N(\mathbf{k}, \mathbf{x}, t)$

$$\frac{\partial}{\partial t} N + \nabla_{\mathbf{x}} \cdot (\dot{\mathbf{x}} N) + \nabla_{\mathbf{k}} \cdot (\dot{\mathbf{k}} N) = S = S_{in} + S_{nl} + S_{ds}, \tag{1}$$

where $\dot{\mathbf{x}} = \partial\omega/\partial\mathbf{k}$ is the group velocity, $\dot{\mathbf{k}} = -\partial\omega/\partial\mathbf{x}$ gives the refraction of ocean waves, and the source functions S represent the physics of wind-wave generation, dissipation by wave breaking and nonlinear four-wave interactions.

It is emphasized that the energy balance equation describes the evolution of the average sea state. Formally, it is obtained by deriving the average evolution of an ensemble of oceans and it assumes that on the short scales of the wave length the wave field is **homogeneous and random**. In this approach it is assumed that the wave components are independent and have random phase. To a good approximation the probability distribution of the ocean surface elevation is Gaussian.

2.1. The source functions

The source functions describe the generation of waves by wind (S_{in}), the dissipation of ocean waves by e.g. wave breaking (S_{diss}) and the energy and momentum conserving resonant four-wave interactions (S_{nl}). A considerable amount of work in the past 50 years has been devoted to the formulation of the source functions.

Nonlinear transfer

The nonlinear interactions, introduced by K. Hasselmann [6], describe the energy transfer between the different wave components in the spectrum. Energy transfer takes place between 4 different waves that satisfy the resonance conditions

$$\omega_1 + \omega_2 = \omega_3 + \omega_4, \ \mathbf{k}_1 + \mathbf{k}_2 = \mathbf{k}_3 + \mathbf{k}_4.$$

Nonlinear interactions play an important role in shaping the spectrum and in freak wave formation. They give rise to an energy cascade through the spectrum. Its representation is known exactly, but is operationally very expensive, therefore an approximation ([7]), called the Direct Interaction Approximation (DIA) is used.

Wind Input

The form of the wind input source function S_{in} was already suggested by Miles [8] in 1957. It depends on the surface stress $\tau = \rho_a u_*^2$ (with ρ_a the air density and u_* the friction velocity) and is proportional to the action density spectrum:

$$S_{in} = \gamma N(\mathbf{k}), \ \frac{\gamma}{\omega} = \epsilon\beta(z_0)\left(\frac{u_* \cos(\theta - \phi)}{c}\right)^2$$

with $c = \omega/k$ the phase speed of the waves, $\epsilon = \rho_a/\rho_w$, and z_0 the roughness length experienced by the airflow.

The wave growth by wind implies a sea-state dependent momentum loss for the airflow [9]. As a consequence, for steep waves the roughness length is larger than for gentle waves. Therefore, in particular for initial growth, there is a strong **mutual interaction** between wind and waves, its strength is determined by the ratio of wave-induced stress τ_w to total kinematic stress τ, with,

$$\tau_w = \rho_w \int \mathrm{d}\mathbf{k} \, \mathbf{k} S_{in}.$$

Dissipation

The dissipation source function describes the reduction of wave momentum and energy caused by processes such as white capping/ wave breaking, the damping by water turbulence, etc. It is modelled in such a way that steep waves experience more dissipation than gentle waves, as steep waves are more likely to break and/or have whitecaps. The breaking waves will give rise to turbulence in the water, resulting in additional mixing of momentum and heat in the upper part of the ocean.

2.2. Energy balance for growing wind waves

The numerical aspects of the action balance equation (1) are presented in WAMDIG [10], [11] and [3]. In this section we discuss the solution of the energy balance equation for the simple case of the generation of ocean waves by wind. To that end we will study the idealized situation of duration-limited wave growth (when a uniform and steady wind has blown over an unlimited ocean for time t after a sudden onset and starting from a flat, calm sea. The case of an unlimited ocean follows when the advection and refraction terms in the action balance equation have been switched off so that one can simulate the duration-limited case by means of a single grid point version of the wave prediction model.

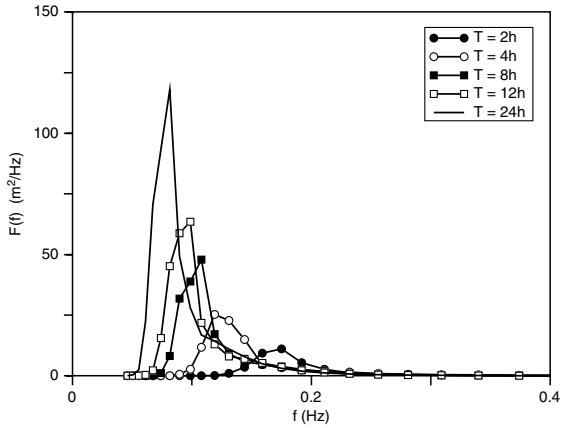

Fig. 1. Evolution of sea state from young windsea (wave age $c_p/u_* \simeq 7$) to older windsea ($c_p/u_* \simeq 25$).

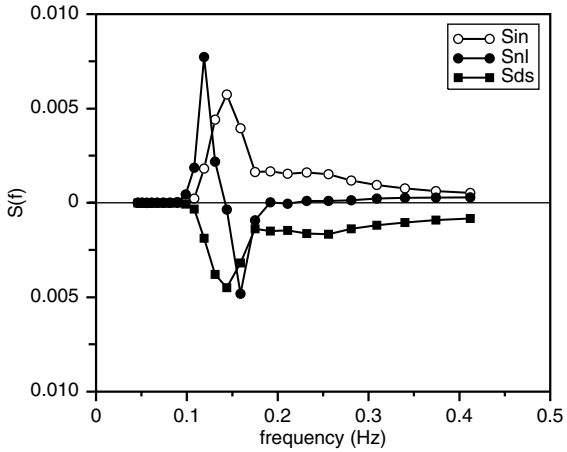

Fig. 2. The energy balance for young wind sea at a duration of 4 h.

In Fig. 1 the evolution in time of the one-dimensional frequency spectrum $F(f)$ over the first 24 hours of the simulation is shown. The stage of development of windsea is usually measured in terms of the wave age parameter

c_p/u_* where c_p is the phase speed of the peak of the spectrum and u_* is the friction velocity which is a measure for the forcing by wind. Typically, for young windsea ($c_p/u_* = 5 - 10$) the waves are strongly forced and steep and the slowing down of wind by the wave-induced stress is large. On the other hand, for old windsea ($c_p/u_* \simeq 25$), the waves are more gentle and weakly forced and the slowing down of the wind by waves is small. This will be discussed in more detail in the section on wind-wave interaction.

The evolution of the simulated frequency spectrum is in accord with the results found during the JONSWAP campaign [12]. In particular, in the course of time a considerable downshift of the peak of the spectrum is seen, corresponding with the generation of longer waves, and, in addition a pronounced overshoot of the peak of the spectrum is noted. Both downshift and overshoot are connected to the action of the nonlinear interactions on the wave spectrum.

In order to better understand the evolution of the gravity wave spectrum we need to study the source functions. To that end, the energy balance equation for young windsea (duration is 4 h corresponding to $c_p/u_* \simeq 12$) is shown in Fig. 2, by plotting the directional averages of S_{in}, S_{nl}, and S_{ds} as function of frequency. Thus, the intermediate frequencies receive energy from the airflow (since S_{in} is positive) which is transported by the nonlinear interactions towards the high and low frequency range. In the high frequency range the nonlinear energy flux maintains an equilibrium spectrum which has an f^{-4} shape, while in the low-frequency range the nonlinear interactions maintain an 'inverse' energy cascade transferring energy towards the region just below the spectral peak, thereby shifting the peak of the spectrum towards lower frequencies. This frequency downshift is to a large extent determined by the shape and the magnitude of the spectral peak itself. For young windsea, having a narrow peak with a considerable peak enhancement, the rate of downshifting is considerable, while for gentle, old windsea this is much less so. In the course of time the peak of the spectrum gradually shifts towards lower frequencies (as may be seen from Fig. 1) until the peak of the spectrum no longer receives input from the wind but instead returns momentum to the airflow because these waves are running faster than the wind. Under these circumstances the waves around the spectral peak are subject to a considerable dissipation so that their steepness reduces. Consequently, because the nonlinear interactions depend on the steepness, the nonlinear transfer is reduced as well, with the result that slowly a quasi-equilibrium spectrum emerges. For old windsea the timescale of downshifting becomes larger than the typical duration of a storm so that for all practical purposes the wind-generated waves evolve towards a steady state.

2.3. Wave forecasting and Validation

A key task in operational wave forecasting is the validation of analysis and forecast against wave observations (see [13]). For reasons of briefness, we concentrate on the verification against buoy data, although there is also very valuable information on the quality of the wave forecasting system by comparison with space borne Altimeter data of significant wave height (see, e.g. [14]. By plotting the verification statistics as function of time, one may monitor the quality of the forecast and analysis system. This shows that there are significant improvements in wave height analysis and forecast over the past 25 years. Spectral shape has improved as well as follows by a comparison with buoy spectra.

It is of course of interest to try to understand the reasons for the improvement in wave height forecast skill over time. Based on extensive experimentation, it turns out that a considerable part ($\approx 75\%$) of the improvement is related to the fact that in the course of time the atmospheric model has improved considerably producing higher quality surface winds. The remainder part of the improvement is caused by wave model improvements such as two-way interaction, better numerics, representation of unresolved bathymetry, a better representation of wave dissipation and increases in spatial and spectral resolution. Also, the use of high quality Altimeter wave height data in the wave analysis has given improvements in wave height forecast skill in particular in the short range forecast.

Let us now present some verification statistics against buoy observations. A wave buoy is basically a float of which the acceleration owing to the surface wave motion is determined. Integrating twice in time then gives the surface elevation signal from which quantities such as the wave energy, frequency spectrum and maximum wave height can be obtained. Note that buoys come in different shapes and sizes and therefore may have a different dynamic range. Thus, there is no garantee that they measure the same wave height. Nevertheless, wave modellers still regard buoys as the ground truth, although there is of course no global coverage.

Fig. 3 shows the results of the verification of analyzed and forecast wave height against buoy data for different forecast ranges over the period of January 1993 until June 2017. The overall trend is that over the years there is a clear reduction in wave height scatter index, defined as the standard deviation of the difference between model and

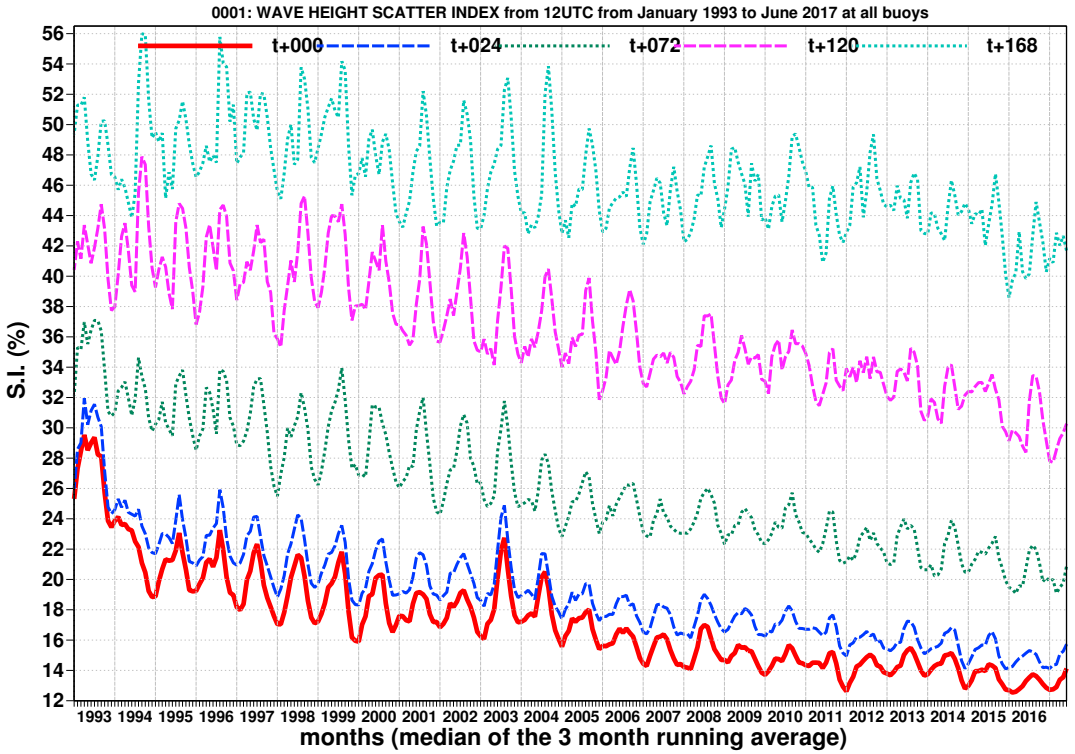

Fig. 3. Evolution of verification statistics for model against buoy data over a 23 year period for analysis and different forecast ranges. In this case the scatter index is shown. Most buoys are located in the Northern hemisphere.

observed wave height, normalized with the mean of observed wave height. In particular, this is the case for the short range forecast up to 5 days ahead, but in the past 5 years there are also definite signs that the medium-range wave forecast is improving as well. As pointed out, an important reason for the improvements in the quality of forecast wave height are better winds. The improvements in wind speed follow from a verification against buoy observations and a more detailed discussion on this topic is given in [15].

The discussion on verification is closed by presenting a relatively new diagnostic tool which enables to study problems in the modelled spectral shape. This is now opportune because a consequence of the large improvements in the forcing wind fields is that it is nowadays more straightforward to identify (systematic) errors in the wave model. This tool was first introduced by [16] in a study to validate SAR and wave model frequency spectra against buoy spectra. One simply determines for each frequency, hence wave period, the wave variance from the modelled and observed frequency spectra in a period bin of, say, two seconds and one obtains the 'equivalent' wave height by the usual definition. The resulting period dependent bias is then plotted as a function of time. In Fig. 4 (see also [17]) an example is given involving all American and Canadian one-dimensional frequency spectra over the period of February 1998 until July 2009. In the range of 10 to 15 seconds there is up to the year 2003 a clear seasonal dependence of the 'equivalent' wave height bias, being large in the summer time and vanishingly small in the winter time.

It turns out that these large positive biases are related to swell events generated by the storms in the Southern Hemisphere winter time. It is tempting to dwell on the causes of the overestimate by the wave model. An obvious candidate would be the dissipation source function, because this source term is the least well-understood. Another candidate is the representation of unresolved islands and atolls. A closer inspection of the verification results revealed that the main problem occurs in the Pacific ocean and not in the Atlantic (not shown). An important difference between the Pacific and the Atlantic ocean is that in the equatorial region of the Pacific there are a vast number of small islands and atolls which are not resolved by the present operational resolution of the wave model. Although these islands are small, they nevertheless block considerable amounts of low-frequency wave energy [18]. Therefore, using a high resolution global topography of 2 minutes, Bidlot (private communication, 2003) determined a wavenumber

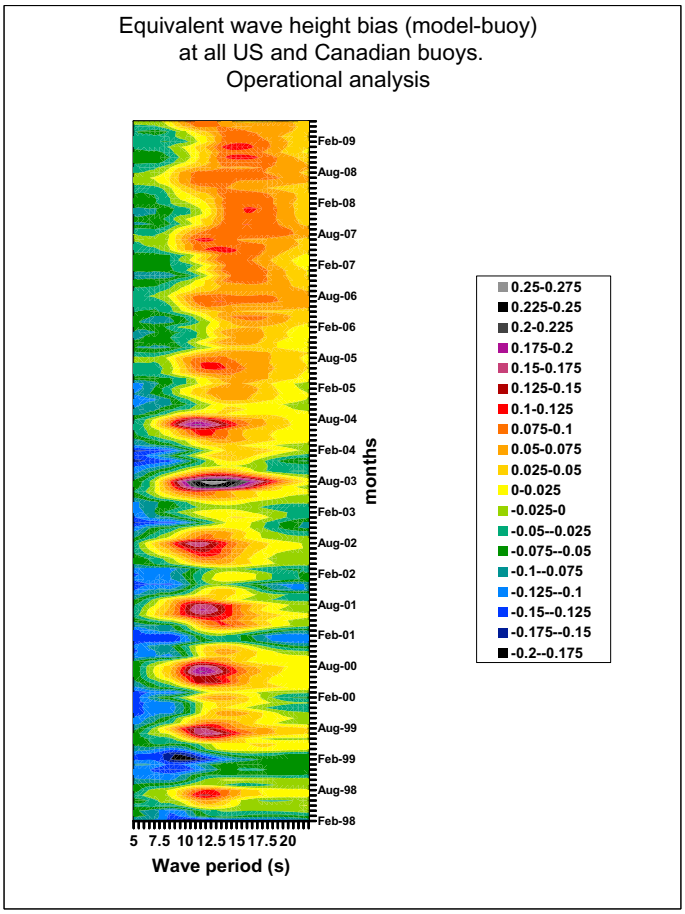

Fig. 4. Spectral bias (model-buoy) at all US and Canadian buos for the period February 1998 until February 2009.

dependent blocking factor. This change was introduced operationally in February 2004 and, as can be seen from Fig. 4, gave a substantial reduction of the bias in the Summer of 2004. Nevertheless, it did not disappear completely.

In March 2005, a new version of the dissipation source function was introduced, which used an alternative definition of the integral parameters, such as mean frequency, in the expression for the dissipation. As can be seen in Fig. 4, this change had a further beneficial impact as in the Summer of 2005 there is virtually no bias anymore in the range of 10 to 15 seconds.

This shows that verification of model forecasts against observations is of vital importance. On the one hand it gives users a good idea of the quality of modelled wave height and spectra, and, on the other hand such an exercise provides modellers important clues to improve the wave prediction system.

3. Wind-Wave Interaction.

In the remainder of this paper we would like to discuss the role of ocean waves in the momentum and heat transfer of a coupled atmosphere-ocean circulation model.

Starting from critical layer theory results are presented on the sea state dependence of the momentum transfer and its impact on the atmospheric circulation and the sea state forecast which is then followed by a discussion of some new results regarding the sea-state dependent heat transfer. Note that in the past (see e.g. [19], [20]) there has been much debate about the use of the critical layer approach in the presence of turbulence. However, field observations of

Hristov *et al.* [21] combined with direct numerical simulations of Sullivan *et al.* [22] have shown that this approach produces realistic results.

3.1. Quasilinear Theory of momentum flux.

According to critical layer theory waves with phase speed c grow when the curvature in the wind profile $U_0(z)$ at the critical height is negative. Introducing the Doppler-shifted velocity $W = U_0(z) - c$, where the critical height z_c follows from the condition $W = 0$, one finds

$$\frac{\partial}{\partial t}F(k)\Big|_{wind} = \gamma F(k),\ \gamma = -\epsilon\pi c\mid\chi_c\mid^2 \frac{W_c''}{\mid W_c'\mid},$$

where the growthrate γ of ocean waves by wind is proportional to the curvature W_c'' in the wind profile (Miles [8]). Here, the wave-induced vertical velocity χ satisfies the Rayleigh equation

$$W\nabla^2\chi - W''\chi = 0,\ \chi(0) = 1,\ \chi(\infty) = 0.$$

Wave growth results in a slowing down of the airflow (see Fabrikant [23] and Janssen [24]) according to

$$\frac{\partial}{\partial t}U_0 = (\nu_a + D_W)\frac{\partial^2}{\partial z^2}U_0 + \frac{1}{\rho_a}\frac{\partial}{\partial z}\tau_{turb},\ D_W = \frac{\pi\omega^2\mid\chi\mid^2}{\mid c - v_g\mid}F(k),$$

where the turbulent stress is modelled by means of a mixing length model, i.e.

$$\tau_{turb} = \rho_a l^2\left|\frac{\partial}{\partial z}U_0\right|\frac{\partial}{\partial z}U_0,\ l(z) = \kappa(z + z_b),$$

while κ is the von Kármán constant and z_b a background roughness length.

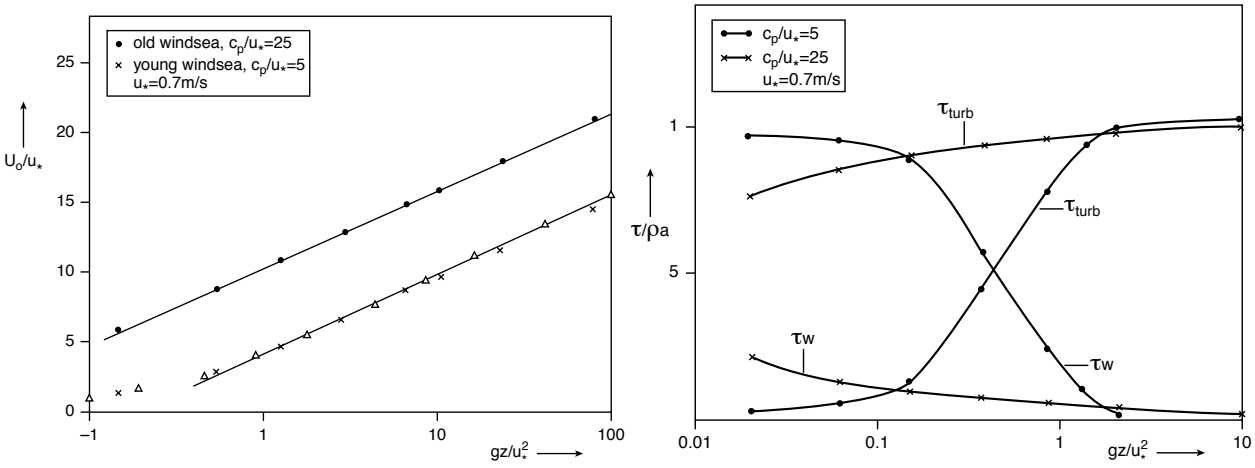

Fig. 5. Left Panel: Effect of waves on wind profile for old and young windsea, shown by plotting dimensionless wind speed U_0/u_* as a function of dimensionless height $z_* = gz/u_*^2$. The wind profile parametrization $1/\kappa\log(1 + z_*/z_0^*)$ is denoted by a $\triangle$. The right Panel shows turbulent stress τ_{turb} and wave stress τ_w as a function of dimensionless height gz/u_*^2 for young and old windsea.

For given spectral shape one may search for steady state solutions of the airflow over wind waves by means of an iteration method. The rate of convergence of this procedure was judged by calculating the total stress $\tau_{tot} = \rho_a u_*^2$

$$\tau_{tot} = \tau_v + \tau_{turb} + \tau_w,$$

where $\tau_v = \rho_a\nu_a\partial U_0/\partial z$ and the wave-induced stress can be shown to be given by

$$\tau_w = -\int_z^\infty \mathrm{d}z D_W\frac{\partial^2}{\partial z^2}U_0 = \int \mathrm{d}\mathbf{k}\ \frac{\partial P}{\partial t}\Big|_{wind}$$

with wave momentum $P = \rho_w g F(\mathbf{k})/c$.

For the actual calculations, reported in [9], the wave spectrum is given by the JONSWAP spectrum with a Phillips parameter α_p which depends in a sensitive manner on the wave age c_p/u_*, i.e.

$$\alpha_p = 0.57(c_p/u_*)^{-3/2},$$

hence young wind waves ($c_p/u_* = 5$) are steep while old wind sea ($c_p/u_* = 25$) is a smooth sea state.

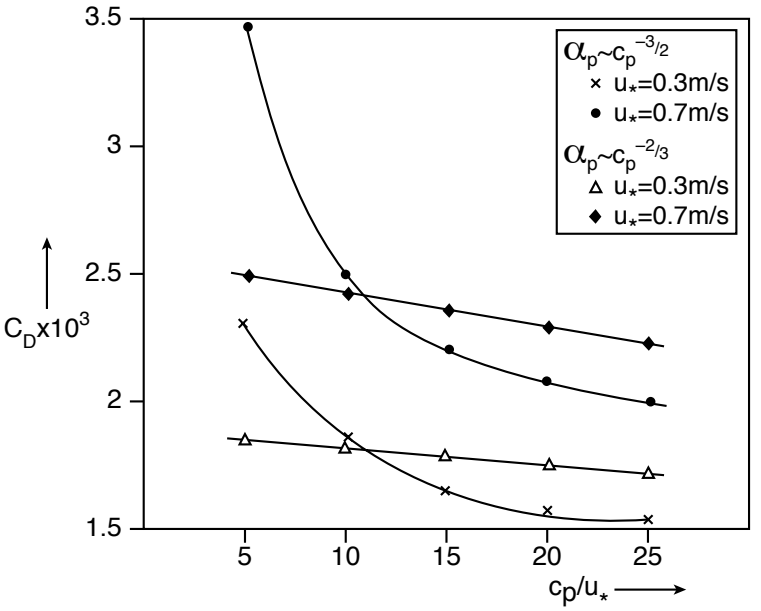

Fig. 6. The wave age dependence of the drag coefficient for two different friction velocities.

The results of the iteration process are given in the Figs. 5 and 6. In the present context the most important result is given in the left panel of Fig. 5. It shows the impact of the sea state on the wind profile. Young waves have a large roughness giving a considerable slowing down of the wind and therefore the equilibrium wind is quite reduced compared to the case of old windsea for which the airflow is much smoother. However, the shape of the wind profile away from the surface still has a logarithmic shape, but close to the surface there are deviations from the logarithmic wind profile, which is a reflection of the impact of growing waves on the wind. This follows immediately from the right panel of Fig. 5 which shows profiles of wave-induced stress and turbulent stress for two different wave ages. For young windsea, the wave-induced stress dominates the total stress near the surface, giving an additional slowing down of the wind, hence a rougher airflow. Finally, Fig. 6 nicely summarizes the effect of growing waves on the wind by showing the dependence of the drag coefficient, defined as $C_D = u_*^2/U_{10}^2$, on the wave age parameter c_p/u_*, which is in good agreement with observations by Donelan [25] and HEXOS [26].

3.2. Parametrization of quasi-linear theory.

The numerical results suggest that air viscosity is not important so for the parametrization we start from the stress relation $\tau_{turb} + \tau_w = \tau$, or explicitely, with $l = \kappa(z + z_b)$[1]

$$l^2 \left| \frac{\partial U_0}{\partial z} \right| \frac{\partial U_0}{\partial z} + \tau_w(z) = \tau.$$

In principle, one could try to solve this differential equation for wind velocity with boundary condition $U_0(z = 0) = 0$ if one knows the wave-induced stress τ_w. However, things turn out to be simpler if one starts from the fit of the

[1] In the original treatment of [2] $l = \kappa z$ and the boundary condition $U_0(z = z_b) = 0$ was specified at $z = z_b$.

wind-profile to the numerical data of [9], which is displayed in the left Panel of Fig. 5,

$$U_0(z) = \frac{u_*}{\kappa} \log\left(1 + \frac{z}{z_0}\right),$$

and determines the τ_w-profile. It is given by

$$\frac{\tau_w(z)}{\tau} = 1 - \frac{(z+z_b)^2}{(z+z_0)^2}$$

Applying the above for $z = 0$, one immediately finds for the roughness length z_0

$$z_0 = \frac{z_b}{\sqrt{1-\tau_w(0)/\tau}} \rightarrow \alpha_{CH} = \frac{g z_0}{u_*^2},$$

with α_{CH} the Charnock parameter. Here, $\tau_w(0)$ at the surface is obtained from the wave model.

Furthermore, from the above one obtains, using the relation $\partial\tau_w/\partial z = D_W \partial^2 U_0/\partial z^2$ an expression for the wave-diffusion coefficient D_W,

$$D_W = 2\kappa u_* \frac{(z+z_b)(z_0-z_b)}{z+z_0}.$$

Another advantage of using the logarithmic wind profile is that it provides a simple parameterization of the wave growth by wind. In order to obtain the growthrate γ one needs to solve the Rayleigh equation which cannot be solved exactly. In stead we use as a starting point an approximate expression for the growth rate that has been obtained by Miles [27] by means of asymptotic matching.

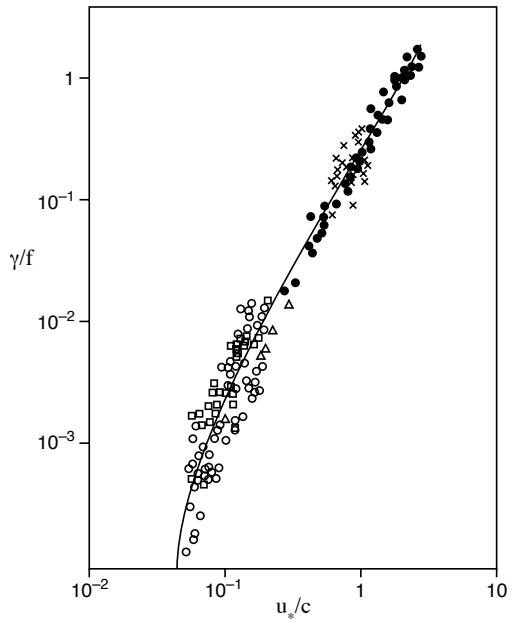

Fig. 7. Comparison of modelled growth rate (with Charnock parameter $\alpha_{CH} = 0.0144$) with observations compiled by Plant [28].

The main result is

$$\gamma/\omega_0 = \epsilon\beta\frac{u_*^2}{c^2},$$

where the Miles' parameter β is given by

$$\beta = \frac{\pi}{\kappa^2} y_c \log^4\left(\frac{y_c}{\lambda}\right), y_c \leq \lambda = \frac{1}{2}e^{-\gamma_E} = 0.281,$$

Here, $y_c = kz_c$ is the dimensionless critical height and ϵ is the air-water density ratio. This expression is valid for slow waves only so in order to have a reasonable approximation also for the long waves, parameters were rescaled by replacing $\lambda = 0.281$ by $\lambda = 1$, and by replacing π by the factor 1.2. In addition, in the formula for the critical height, the parameter u_*/c was shifted by a factor $z_\alpha = 0.08$. As a result the following parametrization for the Miles' parameter β is used:

$$\beta = \frac{1.2}{\kappa^2} y_c \log^4(y_c), y_c \le 1,$$

where

$$y_c = kz_0\left(e^{\kappa/x} - 1\right), \; x = (u_*/c + z_\alpha)\cos(\theta - \phi), z_\alpha = 0.08.$$

The parametrized wave growth is shown in the Fig. 7 and is compared with observations by Plant [28]. Although there is a big scatter in the observations, the agreement of the parametrization with observations seems fair.

3.3. Validation of the approach.

We have performed an extensive validation of the drag coefficient C_D of the coupled ocean-wave, atmosphere system. Two examples are shown in Fig. 8. In the left panel the modelled sea state dependent drag is compared to a parametrization, based on observations from a number of field campaigns, proposed by Huang [29]), which is of the form

$$C_D(\lambda_p/2) = A(c_p/u_*)^a,$$

where λ_p is the peak wavelength, $A = 1.220 \times 10^{-2}$, and $a = -0.704$. The model relation is obtained from one global forecast by averaging $C_D(\lambda_p/2)$ as function of the wave age parameter c_p/u_*. For large wave ages a good agreement between model and observed drag coefficient is obtained while for young windseas there is a some underestimation and there is more scatter. In the right panel of 8 the drag coefficient at 10 m height as function of windspeed U_{10} is

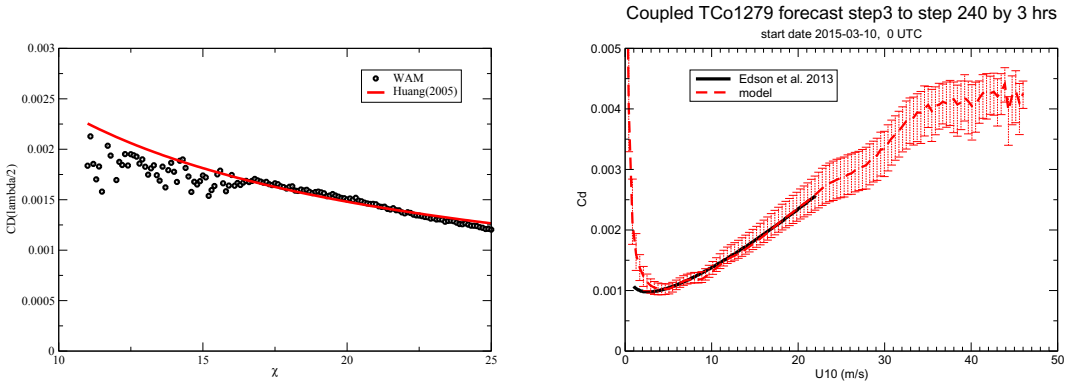

Fig. 8. Left panel compares modelled drag with Huang's [29] emprical relation of sea-state dependent drag coefficient. The right panel compares modelled and observed ([30]) drag coefficient relation with wind speed.

.

validated. The model data are obtained by averaging 80 forecasts of the drag coefficient as function of windspeed. The empirical fit of Edson *et al.* [30] is obtained from eddy correlation data for the COARE 4.0 parametrization of the drag. Noting that this empirical fit is valid up to a wind speed of 23 m/s, it is seen that on average there is a good agreement between modelled drag and observed drag. For extreme, hurricane windspeeds modelled drag shows a tendency to become less sensitive to increases in wind speed, and even shows signs of saturation. This is in qualitative agreement with empirical findings, although it must be emphasized that the scatter in the field observations is large.

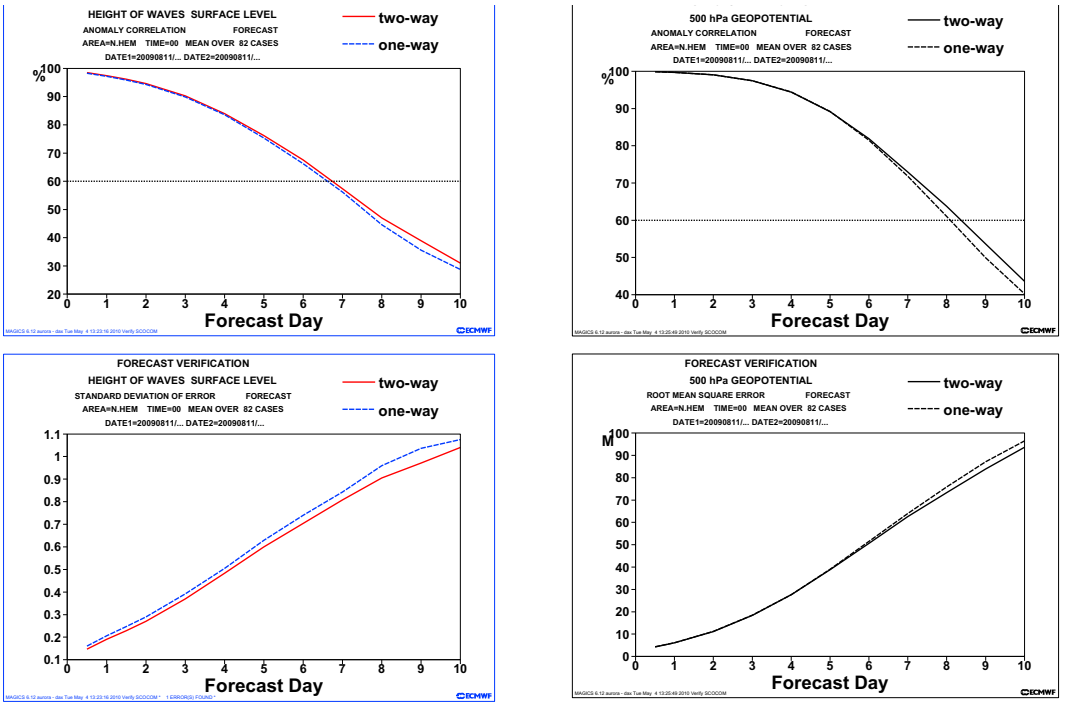

Fig. 9. Left panels show anomaly correlation and standard deviation of error of forecast significant wave height averaged over 82 cases, while the right panel shows the same scores but now for 500 mb geopotential height. Area is the Northern Hemisphere. Coupled forecast is labelled as two-way and no coupling is labelled as one-way.

The next question of interest is whether coupling of wind and waves (two-way interaction for short) has impact on the forecast skill of ocean waves and atmosphere. For medium-range forecasting, evidence that this is indeed the case has been presented by Janssen *et al.* [31] and by Janssen [3], while evidence of impact on the seasonal timescale is given by [32]. Further evidence may be found in Fig. 9. This Figure is based on a comparison of scores of coupled (two-way) and control (one-way) forecasts of significant wave height and 500 mb geopotential height (against the verifying analysis). The number of analyses and 10 day forecasts was 82 and the period was the Summer of 2009. The spatial resolution of the atmospheric component was 40 km while the wave model had a resolution of 28 km. The Figure shows that both near the surface (significant wave height) and in the upper air two-way interaction reduces forecast error and increases the anomaly correlation from 6 days in the forecast.

3.4. Theory and parametrization of heat flux

We have seen that growing ocean waves may have impact on the momentum flux across the air-sea interface. However, it turns out that the sea-state also has a significant impact on the latent and sensible heat flux. In order to see this, the theory of wind-wave generation is extended to include thermal stratification (see for an early account [33]), but the effect of spray as generated by whitecaps and breaking waves is ignored.

In the passive scalar approximation the evolution of mean temperature is found to be

$$\frac{\partial}{\partial t}T_0 = \frac{\partial}{\partial z}\left\{\left(D_w + l^2\left|\frac{\partial U_0}{\partial z}\right| + \delta\nu_z\right)\frac{\partial}{\partial z}T_0\right\}.$$

where it is assumed that close to the surface the heat transport is also determined by molecular conduction, which gives the additional diffusivity $\delta\nu_z$, where δ is a constant of the order of 0.1-0.5.

Assume steady state and introduce the heat flux q_*. Integrating the T-equation one finds

$$\left\{ D_w + l^2 \left| \frac{\partial U_0}{\partial z} \right| + \delta \nu_z \right\} \frac{\partial}{\partial z} T_0 = q_*,$$

which is a differential equation for the air-temperature profile subject to the boundary condition that $T_0(z = 0) = T_S$ with T_S the sea surface temperature.

Using the just found parametrization for the wave diffusion coefficient,

$$D_w = 2\kappa u_* \frac{(z + z_b)(z_0 - z_b)}{z + z_0},$$

and solving the differential equation for $\Delta T = T_a - T_s$ with boundary condition that $\Delta T = 0$ at $z = 0$, gives a logarithmic profile with 'thermal' roughness z_T,

$$\Delta T = \frac{q_*}{\kappa u_*} \log\left(\frac{z}{z_T} \right)$$

where for small $z_\nu = \delta \nu_z / \kappa u_*$ the thermal roughness becomes $z_T = (z_\nu z_0)^{1/2}$.

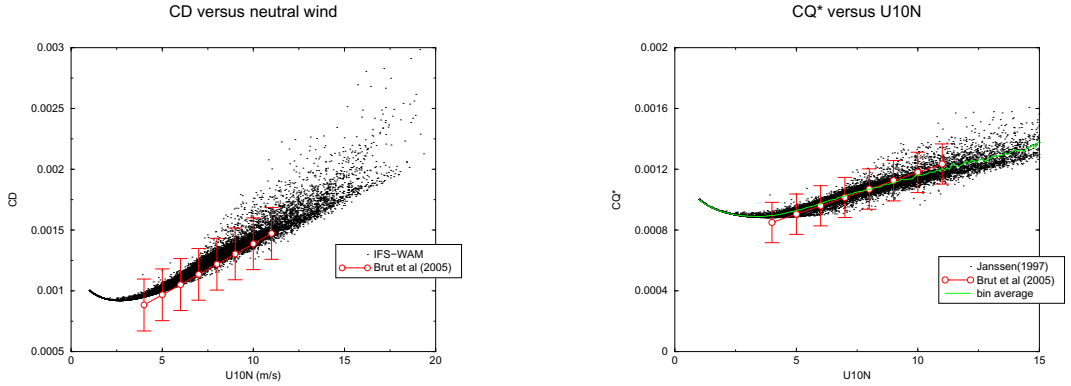

Fig. 10. Comparison of simulated drag coefficient (left panel) and Dalton number (right panel) with empirical fits obtained by Brut *et al.* [34] for the Tropical Atlantic.

Note that by definition $\tau = C_D(10) U_{10}^2$ and $q_* = C_q(10) U_{10} \Delta T_{10}$ so that from the wind and temperature profile one now immediately finds expressions for the drag coefficient C_D and the Dalton number C_q:

$$C_D(10) = \left\{ \frac{\kappa}{\log(10/z_0)} \right\}^2$$

while

$$C_q(10) = \frac{\kappa}{\log(10/z_T)} C_D^{1/2}$$

It is straightforward to evaluate these coefficients from ECMWF's IFS. Results, as shown in Fig. 10 show, in agreement with Brut *et al.* [34], an increase of C_D with wind while C_q also increases with wind but to a lesser extent.

However, the result for C_q is in sharp contrast with HEXOS (De Cosmo *et al.* [35] which suggests a constant for the Dalton number. But, subsequent work by Smedman *et al.* [36] (and also Oost *et al.* [37]) do indicate that C_q increases with wind speed.

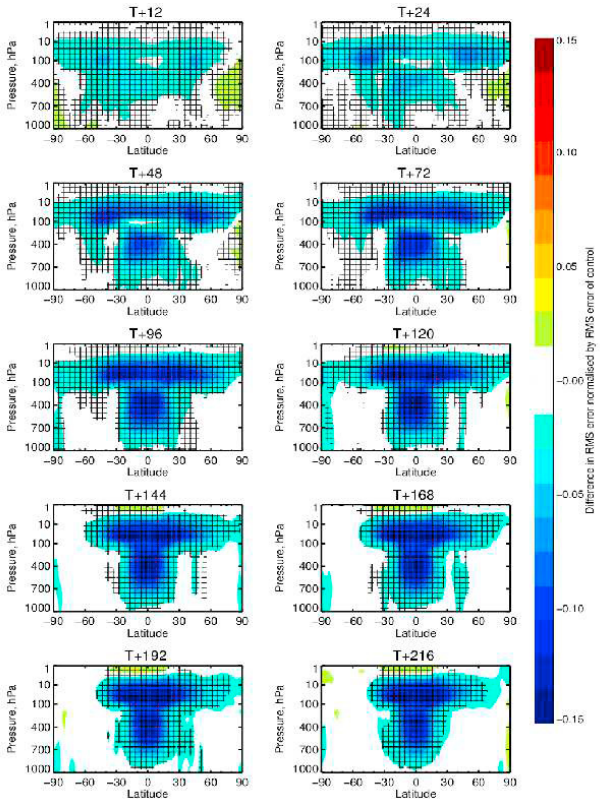

Fig. 11. Zonal mean plots of the impact of the new heat flux parametrization on the relative rms error in geopotential height.

3.5. Impact on Tropical Circulation.

In the past 5-10 years work has been underway to develop a comprehensive coupled forecasting system (atmosphere, ocean-wave, ocean-circulation, and a sea-ice model). It is expected that this system will produce operational deterministic forecasts by the middle of the year 2018.

In the context of this fully coupled system (CY43R1 with resolution TCO 399, corresponding to a spatial resolution of 30 km), we now show impact of the new formulation for the heat flux on the tropical circulation by doing forecasts over a period of one year. The control forecasts were performed with a heat flux formulation that has almost no wind speed dependence. Results of these 10-day forecasts are verified against the operational analysis. As shown in Fig. 11, comparing the verification results for geopotential height shows a significant reduction in forecast error for the experiment with sea-state dependent thermal roughness.

Earlier experiments with a forecast system with fixed SST (so no dynamic ocean) showed much smaller impact, therefore also a dynamic ocean plays an important role in a realistic representation of the Tropical circulation.

4. Conclusions.

Although we have seen that there has been considerable progress in operational wave forecasting over the past 25 years, that does not mean that we are at the end of the journey.

There are still a number of important questions to be solved. For example, the wind-wave interaction approach is extremely simple and might require improvements (essentially it is now one-dimensional theory as vorticity is conserved, effects of vortex stretching need to be included). Furthermore, effects of spray on momentum flux and heat flux need to be incorporated as well.

Also, nonlinear effects such as the generation of second and third harmonics need to be included in a more systematic way, while also the role of ocean waves in upper-ocean mixing (wave breaking and generation of Langmuir turbulence) needs to be better understood. Nevertheless, we are able to give already fairly accurate estimates of the stress (and heatflux) over the oceans.

References

1. Peter A.E.M. Janssen, Øyvind Saetra, Cecilie Wettre, Hans Hersbach and Jean Bidlot, Impact of the sea state on the atmosphere and ocean. *Annales Hydrographiques*, 2004; **3** 3.1-3.23.
2. P.A.E.M. Janssen, Quasi-linear theory of wind wave generation applied to wave forecasting. *J. Phys. Oceanogr.*, 1991; **21** 1631-1642.
3. Peter Janssen, *The Interaction of Ocean Waves and Wind*, 2004, Cambridge University Press, Cambridge, U.K., 300+viiipp.
4. Øyvind Breivik, Kristian Mogensen, Jean-Raymond Bidlot, Magdalena Alonso Balmaseda, Peter A.E.M. Janssen, Surface Wave Effects in the NEMO Ocean Model: Forced and Coupled Experiments. *Journal of Geophysical Research: Oceans* 04/2015; DOI:10.1002/2014JC010565
5. J. Willebrand, Energy transport in a nonlinear and inhomogeneous random gravity wave field, *J. Fluid Mech.*, 1975; **70** 113-126.
6. K. Hasselmann, On the non-linear energy transfer in a gravity-wave spectrum, part 1: general theory, it J. Fluid Mech., 1962; **12** 481.
7. S. Hasselmann, K. Hasselmann, J.H. Allender, T.P. Barnett, Computations and parameterizations of the nonlinear energy transfer in a gravity wave spectrum, part 2: Parameterizations of the nonlinear energy transfer for application in wave models, *J. Phys. Oceanogr.*, 1985; **15** 1378-1391.
8. J.W. Miles, On the generation of surface waves by shear flows. *J. Fluid Mech.*, 1957; **3** 185-204.
9. P.A.E.M. Janssen, Wave-induced stress and the drag of air flow over sea waves, *J. Phys. Oceanogr.*, 1989; **19** 745-754.
10. WAMDI group: S. Hasselmann, K. Hasselmann, E. Bauer, P.A.E.M. Janssen, G.J. Komen, L. Bertotti, P. Lionello, A. Guillaume, V.C. Cardone, J.A. Greenwood, M. Reistad, L. Zambresky and J.A. Ewing, The WAM model - a third generation ocean wave prediction model, *J. Phys. Oceanogr.*, 1988; **18** 1775-1810.
11. G.J. Komen, L. Cavaleri, M. Donelan, K. Hasselmann, S. Hasselmann, and P.A.E.M. Janssen, *Dynamics and Modelling of Ocean waves* 1994, Cambridge University Press, Cambridge, 532 p.
12. K. Hasselmann, T.P. Barnett, E. Bouws, H. Carlson, D.E. Cartwright, K. Enke, J.A. Ewing, H. Gienapp, D.E. Hasselmann, P. Kruseman, A. Meerburg, P. Müller, D.J. Olbers, K. Richter, W. Sell, H. Walden, Measurements of wind-wave growth and swell decay during the Joint North Sea Wave Project (JONSWAP), *Dtsch. Hydrogr. Z.* Suppl. A, 1973; **8**(12), 95p.
13. J.-R. Bidlot, D. J. Holmes, P. A. Wittmann, R. Lalbeharry, H. S. Chen, Intercomparison of the Performance of Operational Ocean Wave Forecasting Systems with Buoy Data, *Weather and Forecasting*, 2002; **17** 287-310.
14. S. Abdalla and P. Janssen, Monitoring Waves and Surface Winds by Satellite Altimetry: Applications, in *Satellite Oceanography over Oceans and Land Surfaces*, 2017; edited by D. Stammer and A. Cazenave, CRC Press, Taylor & Francis group.
15. P.A.E.M. Janssen, Progress in ocean wave forecasting. *Journal of Computational Physics*, 2008; **227** 3572-3594.
16. A.C. Voorrips, C. Mastenbroek, B. Hansen, Validation of two algorithms to retrieve ocean wave spectra from ERS synthetic aperture radar, *J. Geophys. Res.*, 2001; **106** No. C8 16,825-16,840.
17. J.-R. Bidlot, P.A.E.M Janssen, S. Abdalla, On the importance of spectral wave observations in the continued development of global wave models, Proc. Fifth Int. Symposium on Ocean Wave Measurement and Analysis WAVES2005: 3rd-7th July 2005, Madrid, Spain.
18. H.L. Tolman, Treatment of unresolved islands and ice in wind wave models, *Ocean Modelling*,2003; **5** 219-231.
19. D.V. Chalikov and V.K. Makin, Models of the wave boundary layer. *Boundary Layer Meteorol.*,1991; **56** 83-99.
20. S.E. Belcher and J.C.R. Hunt, Turbulent shear flow over slowly moving waves. *J. Fluid Mech.*,1993; **251** 109-148.
21. T.S. Hristov, S.D. Miller, C.A. Friehe, Dynamical coupling of wind and ocean waves through wave-induced air flow, *Nature*, 2003; **442** 55-58.
22. P. Sullivan, J. McWilliams, C.-H. Moeng, Simulation of turbulent flow over idealized water waves, *J. Fluid. Mech.*, 2000; **404** 47-85.
23. A.L. Fabrikant, Quasilinear theory of wind-wave generation. *Izv. Atmos. Ocean. Phys.*,1976; **12** 524-526.
24. P.A.E.M. Janssen, Quasilinear approximation for the spectrum of wind-generated water waves. *J. Fluid Mech.*, 1982; **117** 493-506.
25. M.A. Donelan, The dependence of the aerodynamic drag coefficient on wave parameters, p381-387 in: *Proc. of the first international conference on meteorological and air/sea interaction of the coastal zone*, 1982; Amer. Meteor. Soc., Boston, Mass.
26. S.D. Smith, R.J. Anderson, W.A. Oost, C. Kraan, N. Maat, J. DeCosmo, K.B. Katsaros, K.L. Davidson, K. Bumke, L. Hasse and H.M. Chadwick, Sea surface wind stress and drag coefficients: the HEXOS results. *Boundary Layer Meteorol.*, 1992; **60** 109-142.
27. J.W. Miles, Surface wave generation revisited. *J. Fluid Mech.*, 1993; **256** 427-441.
28. W.J. Plant, A relation between wind stress and wave slope. *J. Geophys. Res.*, 1982; **C87** 1961-1967.
29. P.A. Huang, Temporal and spatial variation of the drag coefficient of a developing sea under steady wind-forcing. *J. Geophys. Res.*, 2005; **110**, C07024. doi:10.1029/2005JC002912
30. J.B. Edson, V. Jampana, R.A. Weller, S.P. Bigorre, A.J. Pluedemann, C.W. Fairall, S.D. Miller, L. Mahrt, D. Vickers and H. Hersbach, On the exchange of Momentum over the Open Ocean, *J. Phys. Oceanogr.*, 2013; **43**, 1378-1391.
31. P.A.E.M. Janssen, J.D. Doyle, J. Bidlot, B. Hansen, L. Isaksen and P. Viterbo, 2002: Impact and feedback of ocean waves on the atmosphere. in *Advances in Fluid Mechanics*, 2002; **33**, Atmosphere-Ocean Interactions ,Vol. I, Ed. W.Perrie.
32. P.A.E.M. Janssen and P. Viterbo, Ocean Waves and the atmospheric Climate. *J. Climate*, 1996; **9** 1269-1287.
33. P.A.E.M. Janssen, Effect of surface gravity waves on the heat flux. ECMWF Technical Memorandum, 1997; no. 239.
34. A. Brut, A. Butet, P. Durand, G. Caniaux and S. Planton, Air-sea exchanges in the equatorial area from the EQUALANT99 dataset: Bulk parametrizations of turbulent fluxes corrected for airflow distortion. *Quarterly Journal of the Royal Meteorological Society*, 2005; **131** 2497-

2538.
35.J. DeCosmo, K. Katsaros, S. Smith, R. Anderson, W. Oost, K. Bumke, and H. Chadwick, Air-sea exchange of water vapor and sensible heat: The Humidity Exchange Over the Sea (HEXOS) results, *J. Geophys. Res.*, 1996; **101(C5)** 12001-12016.
36.Ann-Sofi Smedman, Ulf Sahlée, Erik Högström, and Cecilia Johansson, Critical re-evaluation of the bulk transfer coefficient for sensible heat over the ocean during unstable and neutral conditions. *Quarterly Journal of the Royal Meteorological Society*, 2007; **133** 227-250.
37.W.A. Oost, C.M.J. Jacobs, C. Van Oort, Stability effects on heat and moisture fluxes at sea. *Boundary-Layer Meteorol.*, 2000; **95** 271302.